ACS APPLIED MATERIALS & INTERFACES

Research Article

Cite This: ACS Appl. Mater. Interfaces 2019, 11, 28818−28822

www.acsami.org

Integration of Fullerenes as Electron Acceptors in 3D Graphene Networks: Enhanced Charge Transfer and Stability through Molecular Design

Maira R. Cerón,*[,†] Cheng Zhan,[†] Patrick G. Campbell,[†] Megan C. Freyman,[†] Christy Santoyo,[‡] Luis Echegoyen,[‡] Brandon C. Wood,[†] Juergen Biener,[†] Tuan Anh Pham,[†] and Monika M. Biener*[,†]

[†]Materials Science Division, Lawrence Livermore National Laboratory, 7000 East Avenue, Livermore, California 94550, United States

[‡]Department of Chemistry, University of Texas at El Paso, 500 W University Avenue, El Paso, Texas 79968, United States

Supporting Information

ABSTRACT: Here, we report a concept that allows the integration of the characteristic properties of [60]fullerene in 3D graphene networks. In these systems, graphene provides high electrical conductivity and surface area while fullerenes add high electron affinity. We use molecular design to optimize the interaction between 3D graphene networks and fullerenes, specifically in the context of stability and charge transfer in an electrochemical environment. We demonstrated that the capacity of the 3D graphene network is significantly improved upon the addition of C_{60} and C_{60} monoadducts by providing additional acceptor states in the form of low-lying lowest unoccupied molecular orbitals of C_{60} and its derivative. Guided by experimental results and first-principles calculations, we synthesized and tested a C_{60} monoadduct with increased stability by strengthening the 3D graphene−C_{60} van-der-Waals interactions. The synthesis method and stabilization strategy presented here is expected to benefit the integration of graphene−C_{60} hybrid materials in solar cell and charge storage applications.

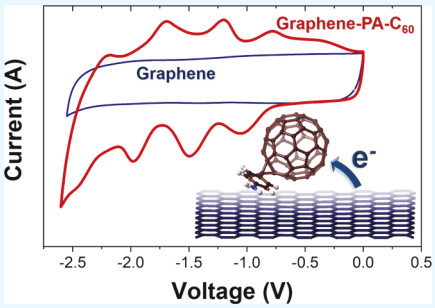

KEYWORDS: *3D graphene network, [60]fullerene, charge transfer, electrochemical stability, capacity*

INTRODUCTION

Graphene and fullerenes are examples of carbon nanomaterials with unique electronic structures and related electrochemical properties that have opened the door to many promising applications in the field of energy storage and harvesting.[1−3] Graphene combines high surface area with high electrical conductivity, which makes it a promising supercapacitor and capacitive desalination material;[1,4−10] fullerenes, on the other hand, are characterized by their high electron affinity which makes them excellent electron acceptors,[11,12] a property that has been exploited for photovoltaics.[2,13−16] C_{60}, in particular, has the ability to store up to 6 electrons in its energetically low-lying triply degenerate lowest unoccupied molecular orbital (LUMO) (i.e., 0.1 electrons per carbon).[11,17,18] For comparison, this is 5−10 times higher than the interfacial capacity of graphene (∼0.01−0.02 electrons per carbon within the electrochemical stability window of water).[7,19−23] In fact, the theoretical charge storage capacitance of [60]fullerene (223 mA h/g) is similar or higher than that of today's standard lithium-ion battery electrode materials (177 mA h/g for $LiFePO_4$).

The challenge, however, is to make fullerenes electrochemically addressable, which requires electrical wiring of individual fullerene molecules. Thus, integrating fullerenes with unique electron acceptor properties in 3D graphene networks with their high surface area and electrical conductivity would be of great benefit for many energy storage and harvesting applications. However, despite their significant potential technological benefits, there are only a few studies about [60]fullerene−graphene hybrids,[24] including as electron extraction layers in polymer solar cells,[25,26] to enhance nonlinear optical performance,[27−32] as well as to facilitate exfoliation of graphite oxide to obtain graphene monolayers.[33] There is clearly a need to shed more light on design and synthesis strategies for graphene−fullerene nanocarbon networks, in order to take advantage of their unique electronic structure.

This work is aimed to achieve a fundamental understanding of the fullerene−graphene interface as it relates to electrochemical stability and charge transfer characteristics. Specifically, we designed, synthesized, and tested a C_{60} monoadduct that allowed us to significantly improve the electrochemical stability of fullerene-functionalized graphene. As an experimental platform, we used binder-free 3D mesoporous graphene macro-assemblies (GMAs) that have exceptionally high surface area (up to 1500 m^2/g) and excellent conductivity (up to 100 S/m).[34−37] Using functionalized C_{60} allowed us to increase the fullerene loading while reducing their tendency to

Received: April 16, 2019
Accepted: July 11, 2019
Published: July 11, 2019

DOI: 10.1021/acsami.9b06681
ACS Appl. Mater. Interfaces 2019, 11, 28818−28822

cluster and to increase the fullerene−graphene physisorption energy whereby increasing the electrochemical stability of the nanocarbon networks. Our experiments were guided by first-principles calculations that provided insights into the performance and stability of the hybrid electrodes.

RESULTSAND DISCUSSION

Cyclic voltammetry (CV) of C_{60} physisorbed on the GMA electrodes[36] in 0.1 M tetrabutylammonium perchlorate in anhydrous acetonitrile shows one C_{60} related reversible reduction peak (the preparation of the GMA-C_{60} nanocarbon composites is described in the Supporting Information. Figure 1a, C_{60} average loading 10 ± 3 wt %). To confirm that the

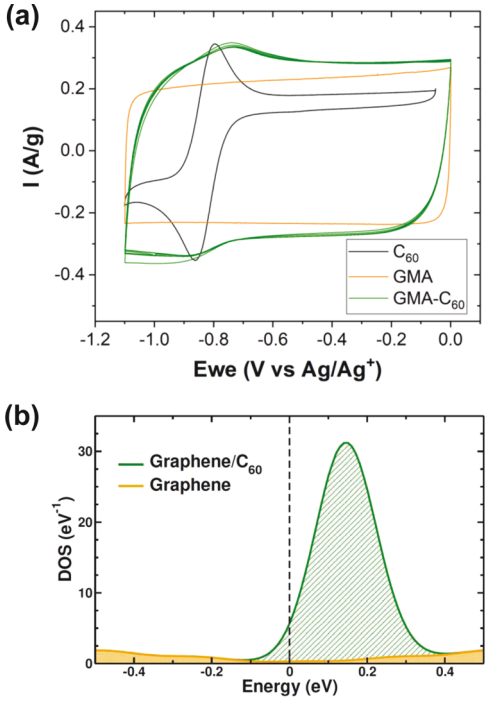

Figure 1. (a) Cyclic voltammogram of the first reduction peak of C_{60} in dichloromethane (black line), GMA in acetonitrile (orange line), and GMA-C_{60} in acetonitrile, 11.2% loading (green line). (b) Total electronic DOS of the graphene−C_{60} electrode (black lines) computed for a model system consisting of one C_{60} molecule and a graphene sheet of 60 carbon atoms. For comparison, the results computed for pristine graphene are also shown (orange lines).

reduction peak observed between −0.8 and −1.1 V originates from the one-electron transfer to C_{60}, we also measured the CV of C_{60} in dichloromethane (Figure 1a, black line, arbitrary units). While the reduction peaks of both CVs are in qualitative agreement, we observed a 60 mV cathodic shift of the C_{60} reduction peak that can be attributed to the characteristic timescale of the charging kinetics of the bulk nanoporous GMA electrode. Although the fullerene loading is only 10%, the gravimetric peak current density of the GMA-C_{60} electrode (Figure 1a, orange line) increased by more than 50%, from 221.3 to 348.5 mA/g. The fraction of C_{60} molecules that can be electrochemically accessed can be calculated by integrating the current peak associated with fullerene charging (Figure 1a) and assuming a charge transfer of one electron per C_{60} (subtracting the underlying GMA charging signal). This analysis reveals that 67% of the C_{60} molecules in the GMA-C_{60} electrodes can be electrochemically accessed (Figure S2, see Supporting Information); the fact that 33% of the deposited C_{60} is electrochemically inaccessible suggests some cluster formation at a length scale below the scanning electron microscopy (SEM) resolution (Figure S3). Note that these C_{60} clusters must have formed during impregnation as we used filtered C_{60} solutions.[38,39]

In order to understand the capacitive performance of the GMA-C_{60} electrodes, we carried out density functional theory (DFT) calculations of C_{60} adsorbed on a single graphene sheet (representing GMA) using the Quantum-ESPRESSO code (see Supporting Information). We focused on the high C_{60} coverage regime, that is, one C_{60} per 60 graphene carbon atoms, that is relevant to the experimental condition. The difference in the charge storage behavior between hybrid and graphene electrodes can be assessed through the calculated electronic density of states (DOS) of the systems. As shown in Figure 1b, the hybrid system exhibits an additional large peak in the DOS just above the Fermi level, which is absent for pristine graphene. This peak originates from the triply degenerate LUMOs of the adsorbed C_{60} molecule and accounts for the experimentally observed reduction peak between −0.8 and −1.1 V that improves the charge storage performance of GMA-C_{60} at negative potentials. By contrast, C_{60} does not induce new features in the occupied DOS within the indicated potential window, and hence little changes are expected in the CVs toward the positive end of the potential sweep, in good agreement with the experiment (Figure 1a).

Functionalization of fullerenes has been successfully used to increase their solubility, allow their characterization, and explore and tune their physical and chemical properties.[13,40,41] Specifically, methanofullerene derivatives are well known for their thermal and electrochemical stability[42] and, as a result, they are often used for the fabrication of solar cells.[16,43] As described above, physisorption of C_{60} on GMA resulted in low fullerene loadings (10 ± 3 wt %), and all attempts to increase the concentration of the C_{60} solutions yielded cluster formation (it is important to note that while C_{60} clusters increase the loading, they cannot be electrochemically addressed due to their large internal resistance).[3,39] To overcome this limitation, we synthesized a more soluble methanofullerene monoadduct, which is less prone to clusters formation. Phenylamine-C_{60} (**PA**-C_{60}) was synthesized using a cyclopropane cycloaddition reaction from a diazo precursor, by in-situ base-induced decomposition of 1-(4-aminophenyl)-ethylidene-*p*-toluenesulfonyl hydrazide in the presence of C_{60}, Figure S1, see Supporting Information.

Physisorption of GMA with **PA**-C_{60} resulted in average loadings of up to 29 ± 4 wt %, almost three times the loading achieved with C_{60}. GMA−**PA**-C_{60} loadings were confirmed by thermogravimetric analysis (TGA). The TGA curves for a 27.5% GMA−**PA**-C_{60} sample (Figure S9) showed a first weight loss at 200 °C, corresponding to decomposition of the cyclopropane addend, followed by a weight loss starting at 500 °C, corresponding to decomposition of the fullerene until reaching 1050 °C,[44−46] where almost no further mass loss was observed. Under our experimental conditions, the TGA curve of GMA−**PA**-C_{60} showed a 47% total mass loss of the initially loaded fullerene, in agreement with the higher thermal stability of the monoadduct **PA**-C_{60} compared to the pristine C_{60}, in which case almost all the initially loaded C_{60} is lost (Figure S4). We also observed a higher decomposition temperature of the fullerene from 360 °C for the pure **PA**-C_{60} to 500 °C for the hybrid GMA−**PA**-C_{60}. This can be understood on the basis

DOI: 10.1021/acsami.9b06681
ACS Appl. Mater. Interfaces 2019, 11, 28818−28822

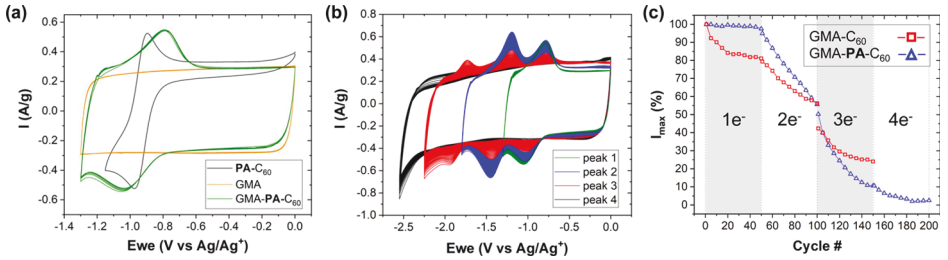

Figure 2. (a) Cyclic voltammogram of the first reduction peak of **PA**-C_{60} in dichloromethane (black line), GMA in acetonitrile (orange line), and GMA−**PA**-C_{60} in acetonitrile, 30.00% loading (green line). (b) Cycling voltammogram of GMA−**PA**-C_{60} at different potential windows. (c) Comparison of cycling stability of GMA-C_{60} and GMA−**PA**-C_{60}. The I_{max} value is derived from CVs at different potential windows covering 1, 2, 3, or 4 electron transfers.

of the large number of wall contacts involved in diffusion through a bulk nanoporous material where even small changes in the van der Waals interaction can delay desorption by increasing the accumulative wall residence time.

CVs of GMA−**PA**-C_{60} in the potential window from 0 to −1.3 V reveals that the position of the first reduction peak of **PA**-C_{60} is negatively shifted, approximately 150 mV, compared to that for GMA-C_{60} under the same experimental conditions (Figure 2a), consistent with previous reports of cathodic shifts upon double-bond removal by chemical functionalization.[47−49] In addition, good agreement was found between the CVs obtained from GMA−**PA**-C_{60} and **PA**-C_{60} in dichloromethane, an indication that the observed reduction peak originates from one-electron transfer into the C_{60} monoadduct. The ∼100 mV cathodic shift of the **PA**-C_{60} reduction peak potential again reflects the characteristic charging kinetics of the bulk nanoporous GMA electrode. Remarkably, the functionalization with **PA**-C_{60} doubles the gravimetric peak current density of the GMA electrode (Figure 2a, orange line), from 272.2 to 548.6 mA/g. A detailed analysis reveals that, despite the high **PA**-C_{60} loading, 82% of the physisorbed **PA**-C_{60} molecules was electrochemically accessed (Figure S2). These results clearly demonstrate that functionalization of C_{60} is an effective strategy to decrease cluster formation and increase fullerene solubility.

Cyclic voltammograms of GMA−**PA**-C_{60} at different potential sweep rates allowed us to calculate the charge transfer utilization of GMA−**PA**-C_{60} as a function of the scan rate (Figures S10 and S11). We observed a slight decrease of the performance of GMA−**PA**-C_{60} upon increasing the scan rate. The negative (cathodic) shift of the **PA**-C_{60} related charging peak with the increasing scan rate suggests that some solution resistance was not fully compensated, thus preventing the complete charging of **PA**-C_{60} at higher scan rates within the applied potential window.

Figure 2b/c shows a significantly higher cycling stability of GMA−**PA**-C_{60} compared to GMA-C_{60} when only 1 electron per fullerene molecule is introduced to the system. The electrochemical stability of physisorbed fullerenes depends, among other factors, on their solubility and the graphene−fullerene physisorption energy. The latter is expected to decrease with increasing electron transfer into the C_{60} LUMOs, which leads to electrostatic repulsion between negatively charged graphene sheets and fullerene molecules (see discussion below). Interestingly, the stability trend **PA**-C_{60} > C_{60} observed for the first electron transfer (C_{60} to C_{60}^{-}) remains the same for the second electron transfer (C_{60}^{-} to C_{60}^{2-}) but is reversed for the third electron transfer (C_{60}^{2-} to C_{60}^{3-}). As demonstrated in a previous study,[50] the added negative charge is localized in the C_{60} adsorbate. In this regard, the overall decreasing stability of physisorbed C_{60} with increasing charge transfer can be qualitatively understood in terms of the increasingly repulsive interactions between the negatively charged C_{60} adsorbate and the graphene substrate. Accordingly, accessing higher C_{60} charging states (theoretically up to C_{60}^{6-}) will require functionalization with more stable, covalently bonded C_{60} derivates.

We calculated the binding energy of C_{60} and **PA**-C_{60} with the graphene substrate to investigate the stability of the fullerene−graphene hybrid electrodes. In particular, we performed classical molecular dynamic (CMD) simulations to efficiently explore the most stable configurations of C_{60} and **PA**-C_{60} on graphene (see Supporting Information).[51] These configurations were then re-optimized and used for binding energy calculations with DFT, which provides a more accurate description of molecular interactions in the systems. Analysis of the representative configurations (Figure 3) derived from

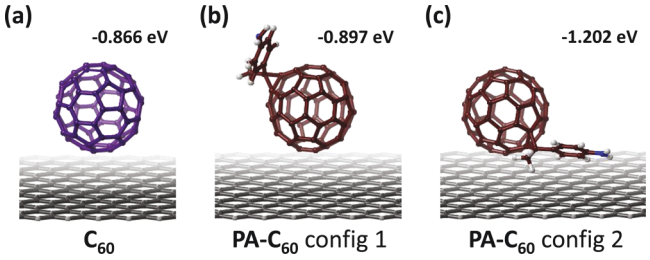

Figure 3. Binding configurations of fullerene−graphene hybrids (a) C_{60}−graphene. (b) **PA**-C_{60}−graphene with the addend pointing away from the graphene. (c) **PA**-C_{60}−graphene with the addend close to the graphene.

CMD simulations shows that the functional group significantly enhances the bonding strength between **PA**-C_{60} and graphene when being close to the substrate. This behavior stems from the $\pi-\pi$ interaction between the addend and graphene,[52−54] resulting in a 0.3 eV increase of the binding energy between **PA**-C_{60} and graphene compared to that of C_{60}. Collectively, these simulation results are consistent with TGA and CV measurements, indicating the important role of the functional group in determining the stability of the hybrid electrode.

CONCLUSIONS

To summarize, we present a detailed investigation of the electrochemical charging behavior of fullerene−graphene electrodes using a combination of experiments and first-principles calculations. When compared to pristine graphene, we find that the capacity of the system is significantly improved

DOI: 10.1021/acsami.9b06681
ACS Appl. Mater. Interfaces 2019, 11, 28818−28822

upon the addition of C_{60} and C_{60} monoadducts by providing additional acceptor states in the form of the low-lying LUMOs of C_{60} and its derivate. We also showed that the design of the C_{60} monoadduct plays a key role in the electrochemical performance of the hybrid electrode. Specifically, increasing the solubility of C_{60} improved the C_{60} loading and reduced cluster formation; the latter enhances the electrochemical accessibility of fullerene and thus warrants its utilization. Finally, functionalization of C_{60} considerably improves the cycling stability of the hybrid material due to the additional $\pi-\pi$ interaction between the addend and graphene, thus allowing access of charging states up to C_{60}^{3-}. This trend was confirmed by DFT calculations of the binding energies of C_{60} and C_{60} monoadducts on graphene. The stabilization strategy presented in this work is ideally suited for applications that are dominated by one-electron transfer such as those in photovoltaic solar cells. Further optimization of the hybrid system using, for example, covalently bonded fullerene−graphene may provide even higher electrochemical stability, thus benefiting energy storage applications.

■ ASSOCIATED CONTENT

Supporting Information

The Supporting Information is available free of charge on the ACS Publications website at DOI: 10.1021/acsami.9b06681.

Detailed description of the synthesis and characterization of fullerene derivatives and fullerene−3D graphene networks as well as computational details (PDF)

■ AUTHOR INFORMATION

Corresponding Authors

*E-mail: ceronhernand1@llnl.gov (M.R.C.).
*E-mail: biener3@llnl.gov (M.M.B.).

ORCID

Maira R. Cerón: 0000-0002-5151-0479
Patrick G. Campbell: 0000-0003-0167-4624
Luis Echegoyen: 0000-0003-1107-9423
Tuan Anh Pham: 0000-0003-0025-7263
Monika M. Biener: 0000-0001-7289-5905

Author Contributions

The manuscript was written through contributions of all the authors. All the authors have given approval to the final version of the manuscript.

Notes

The authors declare no competing financial interest.

■ ACKNOWLEDGMENTS

This work was performed under the auspices of the U.S. Department of Energy by Lawrence Livermore National Laboratory under Contract DE-AC52-07NA27344. Funding was provided by the Lawrence Livermore National Laboratory Directed Research and Development (LDRD) Grant 17-ERD-017. IM release: LLNL-JRNL-768044. Mass spectrometric measurements at the Molecular Foundry was supported by the Office of Science, Office of Basic Energy Sciences, of the U.S. Department of Energy under contract no. DE-AC02-05CH11231. L.E. acknowledges the National Science Foundation, grants CHE-1801317 for generous support. L.E. also thanks the Robert A. Welch Foundation for an endowed chair grant AH-0033. The authors thank Ryan Chen for the covert art design.

■ ABBREVIATIONS

GMA, graphene macro-assemblies
LUMO, lowest unoccupied molecular orbital
SEM, scanning electron microscopy
vdW, van der Waals
TGA, thermogravimetric analysis
CV, cyclic voltammetry
DFT, density functional theory
CMD, classical molecular dynamics

■ REFERENCES

(1) Jiang, H.; Lee, P. S.; Li, C. 3d Carbon Based Nanostructures for Advanced Supercapacitors. *Energy Environ. Sci.* **2013**, *6*, 41−53.
(2) Fang, Y.; Bi, C.; Wang, D.; Huang, J. The Functions of Fullerenes in Hybrid Perovskite Solar Cells. *ACS Energy Lett* **2017**, *2*, 782−794.
(3) Campbell, P. G.; Merrill, M. D.; Wood, B. C.; Montalvo, E.; Worsley, M. A.; Baumann, T. F.; Biener, J. Battery/Supercapacitor Hybrid Via Non-Covalent Functionalization of Graphene Macro-Assemblies. *J. Mater. Chem. A* **2014**, *2*, 17764−17770.
(4) Simon, P.; Gogotsi, Y. Materials for Electrochemical Capacitors. *Nat. Mater.* **2008**, *7*, 845−854.
(5) Gogotsi, Y.; Nikitin, A.; Ye, H.; Zhou, W.; Fischer, J. E.; Yi, B.; Foley, H. C.; Barsoum, M. W. Nanoporous Carbide-Derived Carbon with Tunable Pore Size. *Nat. Mater.* **2003**, *2*, 591−594.
(6) Zhang, L. L.; Zhao, X. S. Carbon-Based Materials as Supercapacitor Electrodes. *Chem. Soc. Rev.* **2009**, *38*, 2520−2531.
(7) Zhai, Y.; Dou, Y.; Zhao, D.; Sheng, D. Carbon Materials for Chemical Capacitive Energy Storage. *Adv. Mater.* **2011**, *23*, 4828−4850.
(8) Simon, P.; Gogotsi, Y. Capacitive Energy Storage in Nanostructured Carbon-Electrolyte Systems. *Acc. Chem. Res.* **2013**, *46*, 1094−1103.
(9) Hawks, S. A.; Knipe, J. M.; Campbell, P. G.; Loeb, C. K.; Hubert, M. A.; Santiago, J. G.; Stadermann, M. Quantifying the Flow Efficiency in Constant-Current Capacitive Deionization. *Water Res.* **2018**, *129*, 327−336.
(10) Feng, X.; Zhao, J.; Sun, D.; Shanmugam, L.; Kim, J.-K.; Yang, J. Novel Onion-Like Graphene Aerogel Beads for Efficient Solar Vapor Generation under Non-Concentrated Illumination. *J. Mater. Chem. A* **2019**, *7*, 4400−4407.
(11) Echegoyen, L.; Echegoyen, L. E. Electrochemistry of Fullerenes and Their Derivatives. *Acc. Chem. Res.* **1998**, *31*, 593−601.
(12) Guldi, D. M. Fullerenes: Three Dimensional Electron Acceptor Materials. *Chem. Commun.* **2000**, 321−327.
(13) Montellano Lopez, A.; Mateo-Alonso, A.; Prato, M., Fullerenes for Materials Science. *Fullerenes: Principles and Applications (2)*; The Royal Society of Chemistry, 2012; pp 389−413, Chapter 11.
(14) Hudhomme, P.; Cousseau, J. Fullerene Derivatives for Organic Photovoltaics. *Fullerenes: Principles and Applications (2)*; The Royal Society of Chemistry, 2012; pp 416−461, Chapter 12.
(15) Bianco, A.; Da Ros, T. Biological Applications of Fullerenes. *Fullerenes: Principles and Applications (2)*; The Royal Society of Chemistry, 2012; pp 507−545, Chapter 14.
(16) Mishra, A.; Bäuerle, P. Small Molecule Organic Semiconductors on the Move: Promises for Future Solar Energy Technology. *Angew. Chem., Int. Ed.* **2012**, *51*, 2020−2067.
(17) Ma, J.; Guo, Q.; Gao, H.-L.; Qin, X. Synthesis of C60/Graphene Composite as Electrode in Supercapacitors. *Fullerenes, Nanotubes, Carbon Nanostruct.* **2015**, *23*, 477−482.
(18) Kouloumpis, A.; Spyrou, K.; Dimos, K.; Georgakilas, V.; Rudolf, P.; Gournis, D. A Bottom-up Approach for the Synthesis of Highly Ordered Fullerene-Intercalated Graphene Hybrids. *Front. Mater.* **2015**, *2*, DOI: 10.3389/fmats.2015.00010.

(19) Wood, B. C.; Ogitsu, T.; Otani, M.; Biener, J. First-Principles-Inspired Design Strategies for Graphene-Based Supercapacitor Electrodes. *J. Phys. Chem. C* **2014**, *118*, 4−15.
(20) Stoller, M. D.; Magnuson, C. W.; Zhu, Y.; Murali, S.; Suk, J. W.; Piner, R.; Ruoff, R. S. Interfacial Capacitance of Single Layer Graphene. *Energy Environ. Sci.* **2011**, *4*, 4685−4689.
(21) Ji, H.; Zhao, X.; Qiao, Z.; Jung, J.; Zhu, Y.; Lu, Y.; Zhang, L. L.; MacDonald, A. H.; Ruoff, R. S. Capacitance of Carbon-Based Electrical Double-Layer Capacitors. *Nat. Commun.* **2014**, *5*, 3317.
(22) Zhan, C.; Neal, J.; Wu, J.; Jiang, D.-e. Quantum Effects on the Capacitance of Graphene-Based Electrodes. *J. Phys. Chem. C* **2015**, *119*, 22297−22303.
(23) Paek, E.; Pak, A. J.; Hwang, G. S. A Computational Study of the Interfacial Structure and Capacitance of Graphene in [Bmim][Pf6] Ionic Liquid. *J. Electrochem. Soc.* **2013**, *160*, A1−A10.
(24) Guan, J.; Chen, X.; Wei, T.; Liu, F.; Wang, S.; Yang, Q.; Lu, Y.; Yang, S. Directly Bonded Hybrid of Graphene Nanoplatelets and Fullerene: Facile Solid-State Mechanochemical Synthesis and Application as Carbon-Based Electrocatalyst for Oxygen Reduction Reaction. *J. Mater. Chem. A* **2015**, *3*, 4139−4146.
(25) Tung, V. C.; Huang, J.-H.; Tevis, I.; Kim, F.; Kim, J.; Chu, C.-W.; Stupp, S. I.; Huang, J. Surfactant-Free Water-Processable Photoconductive All-Carbon Composite. *J. Am. Chem. Soc.* **2011**, *133*, 4940−4947.
(26) Qu, S.; Li, M.; Xie, L.; Huang, X.; Yang, J.; Wang, N.; Yang, S. Noncovalent Functionalization of Graphene Attaching [6,6]-Phenyl-C61-Butyric Acid Methyl Ester (Pcbm) and Application as Electron Extraction Layer of Polymer Solar Cells. *ACS Nano* **2013**, *7*, 4070−4081.
(27) Zhang, X.; Huang, Y.; Wang, Y.; Ma, Y.; Liu, Z.; Chen, Y. Synthesis and characterization of a graphene-C60 hybrid material. *Carbon* **2009**, *47*, 334−337.
(28) Liu, Z.-B.; Xu, Y.-F.; Zhang, X.-Y.; Zhang, X.-L.; Chen, Y.-S.; Tian, J.-G. Porphyrin and Fullerene Covalently Functionalized Graphene Hybrid Materials with Large Nonlinear Optical Properties. *J. Phys. Chem. B* **2009**, *113*, 9681−9686.
(29) Zhang, X.; Liu, Z.; Huang, Y.; Wan, X.; Tian, J.; Ma, Y.; Chen, Y. Synthesis, Characterization and Nonlinear Optical Property of Graphene-C60 Hybrid. *J. Nanosci. Nanotechnol.* **2009**, *9*, 5752−5756.
(30) Ullmann, K.; Coto, P. B.; Leitherer, S.; Molina-Ontoria, A.; Martín, N.; Thoss, M.; Weber, H. B. Single-Molecule Junctions with Epitaxial Graphene Nanoelectrodes. *Nano Lett.* **2015**, *15*, 3512−3518.
(31) Garrido, M.; Calbo, J.; Rodríguez-Pérez, L.; Aragó, J.; Ortí, E.; Herranz, M. Á.; Martín, N. Non-Covalent Graphene Nanobuds from Mono- and Tripodal Binding Motifs. *Chem. Commun.* **2017**, *53*, 12402−12405.
(32) García, D.; Rodríguez-Pérez, L.; Herranz, M. A.; Peña, D.; Guitián, E.; Bailey, S.; Al-Galiby, Q.; Noori, M.; Lambert, C. J.; Pérez, D.; Martín, N. A C_{60}-Aryne Building Block: Synthesis of a Hybrid All-Carbon Nanostructure. *Chem. Commun.* **2016**, *52*, 6677−6680.
(33) Zhang, Y.; Ren, L.; Wang, S.; Marathe, A.; Chaudhuri, J.; Li, G. Functionalization of Graphene Sheets through Fullerene Attachment. *J. Mater. Chem.* **2011**, *21*, 5386−5391.
(34) Worsley, M. A.; Pauzauskie, P. J.; Olson, T. Y.; Biener, J.; Satcher, J. H.; Baumann, T. F. Synthesis of Graphene Aerogel with High Electrical Conductivity. *J. Am. Chem. Soc.* **2010**, *132*, 14067−14069.
(35) Worsley, M. A.; Olson, T. Y.; Lee, J. R. I.; Willey, T. M.; Nielsen, M. H.; Roberts, S. K.; Pauzauskie, P. J.; Biener, J.; Satcher, J. H.; Baumann, T. F. High Surface Area, Sp2-Cross-Linked Three-Dimensional Graphene Monoliths. *J. Phys. Chem. Lett.* **2011**, *2*, 921−925.
(36) Worsley, M. A.; Kucheyev, S. O.; Mason, H. E.; Merrill, M. D.; Mayer, B. P.; Lewicki, J.; Valdez, C. A.; Suss, M. E.; Stadermann, M.; Pauzauskie, P. J.; Satcher, J. H.; Biener, J.; Baumann, T. F. Mechanically Robust 3d Graphene Macroassembly with High Surface Area. *Chem. Commun.* **2012**, *48*, 8428−8430.
(37) Biener, J.; Dasgupta, S.; Shao, L.; Wang, D.; Worsley, M. A.; Wittstock, A.; Lee, J. R. I.; Biener, M. M.; Orme, C. A.; Kucheyev, S. O.; Wood, B. C.; Willey, T. M.; Hamza, A. V.; Weissmüller, J.; Hahn, H.; Baumann, T. F. Macroscopic 3d Nanographene with Dynamically Tunable Bulk Properties. *Adv. Mater.* **2012**, *24*, 5083−5087.
(38) Ruoff, R. S.; Tse, D. S.; Malhotra, R.; Lorents, D. C. Solubility of Fullerene (C60) in a Variety of Solvents. *J. Phys. Chem.* **1993**, *97*, 3379−3383.
(39) Zhang, P.; Lu, J.; Xue, Q.; Liu, W. Microfrictional Behavior of C60Particles in Different C60LB Films Studied by AFM/FFM. *Langmuir* **2001**, *17*, 2143−2145.
(40) Hawkins, J. M.; Lewis, T. A.; Loren, S. D.; Meyer, A.; Heath, J. R.; Shibato, Y.; Saykally, R. J. Organic Chemistry of C_{60} (Buckminsterfullerene): Chromatography and Osmylation. *J. Org. Chem.* **1990**, *55*, 6250−6252.
(41) Caballero, R.; de la Cruz, P.; Langa, F. Basic Principles of the Chemical Reactivity of Fullerenes. *Fullerenes: Principles and Applications (2)*; The Royal Society of Chemistry, 2012; pp 66−124, Chapter 3.
(42) Cerón, M. R.; Izquierdo, M.; Aghabali, A.; Valdez, J. A.; Ghiassi, K. B.; Olmstead, M. M.; Balch, A. L.; Wudl, F.; Echegoyen, L. Tethered Bisadducts of C_{60} and C_{70} with Addends on a Common Hexagonal Face and a 12-Membered Hole in the Fullerene Cage. *J. Am. Chem. Soc.* **2015**, *137*, 7502−7508.
(43) Thompson, B. C.; Fréchet, J. M. J. Polymer-Fullerene Composite Solar Cells. *Angew. Chem., Int. Ed.* **2008**, *47*, 58−77.
(44) Crumpton, D. M.; Laitinen, R. A.; Smieja, J.; Cleary, D. A. Thermal Analysis of Carbon Allotropes: An Experiment for Advanced Undergraduates. *J. Chem. Edu.* **1996**, *73*, 590.
(45) Sundar, C. S.; Bharathi, A.; Hariharan, Y.; Janaki, J.; Sankara Sastry, V.; Radhakrishnan, T. S. Thermal Decomposition of C_{60}. *Solid State Commun.* **1992**, *84*, 823−826.
(46) Cataldo, F. A Study on the Thermal Stability to 1000°C of Various Carbon Allotropes and Carbonaceous Matter Both under Nitrogen and in Air. *Fullerenes, Nanotubes, Carbon Nanostruct.* **2002**, *10*, 293−311.
(47) Carano, M.; Marcaccio, M.; Paolucci, F. Three Electrodes and a Cage: An Account of Electrochemical Research on C_{60}, C_{70} and Their Derivatives. In *Fullerenes: Principles and Applications (2)*; The Royal Society of Chemistry, 2012; pp 237−269, Chapter 7.
(48) Kessinger, R.; Fender, N. S.; Echegoyen, L. E.; Thilgen, C.; Echegoyen, L.; Diederich, F. Selective Electrolytic Removal of Bis(Alkoxycarbonyl)Methano Addends from C_{60} Bis-Adducts and Electrochemical Stability of C_{70} Derivatives. *Chem.—Eur. J.* **2000**, *6*, 2184−2192.
(49) Deng, F.; Wang, G.-W.; Zhang, T.-H.; Jiao, L.-J.; Chen, S. Ligand Effects on the Electrochemical and Spectroscopic Behaviors of Methano[60]Fullerene Derivatives. *Chem. Commun.* **2004**, *9*, 1118−1119.
(50) Zhan, C.; Pham, T. A.; Cerón, M. R.; Campbell, P. G.; Vedharathinam, V.; Otani, M.; Jiang, D.-e.; Biener, J.; Wood, B. C.; Biener, M. Origins and Implications of Interfacial Capacitance Enhancements in C_{60}-Modified Graphene Supercapacitors. *ACS Appl. Mater. Interfaces* **2018**, *10*, 36860−36865.
(51) Ojeda-Aristizabal, C.; Santos, E. J. G.; Onishi, S.; Yan, A.; Rasool, H. I.; Kahn, S.; Lv, Y.; Latzke, D. W.; Velasco, J.; Crommie, M. F.; Sorensen, M.; Gotlieb, K.; Lin, C.-Y.; Watanabe, K.; Taniguchi, T.; Lanzara, A.; Zettl, A. Molecular Arrangement and Charge Transfer in C_{60}/Graphene Heterostructures. *ACS Nano* **2017**, *11*, 4686−4693.
(52) Li, K.; Li, H.; Yan, N.; Wang, T.; Zhao, Z. Adsorption and Dissociation of Ch_4 on Graphene: A Density Functional Theory Study. *Appl. Surf. Sci.* **2018**, *459*, 693−699.
(53) AlZahrani, A. Z. First-Principles Study on the Structural and Electronic Properties of Graphene Upon Benzene and Naphthalene Adsorption. *Appl. Surf. Sci.* **2010**, *257*, 807−810.
(54) Zhang, Y.-H.; Chen, Y.-B.; Zhou, K.-G.; Liu, C.-H.; Zeng, J.; Zhang, H.-L.; Peng, Y. Improving Gas Sensing Properties of Graphene by Introducing Dopants and Defects: A First-Principles Study. *Nanotechnology* **2009**, *20*, 185504.

DOI: 10.1021/acsami.9b06681
ACS Appl. Mater. Interfaces 2019, 11, 28818−28822